Progress In Electromagnetics Research C, Vol. 63, 173–182, 2016

The Image Phase Approach for the Design of RF MEMS Shunt Switches

Giancarlo Bartolucci[1, *], Giorgio De Angelis[2], Andrea Lucibello[3], Romolo Marcelli[3], and Emanuela Proietti[3]

Abstract—In this paper a new method to solve the microwave matching problem of MEMS shunt connected switches is proposed, as an extension of a previously presented approach based on the image parameter formulation. The image phase concept is used to impose the matching condition in the "ON" state of the device, which is the most critical one. Two different configurations are investigated: a single basic cell and double basic cell topologies. For both of them an analytic modeling procedure is developed, and the equations for the synthesis of the structures are derived. In order to provide some examples, the method has been applied to a previously realized MEMS shunt variable capacitor.

1. INTRODUCTION

RF MEMS coplanar waveguide (CPW) shunt connected capacitive switches are two state devices typically composed by a metal bridge which is actuated by means of a bias voltage [1–7]. The "UP" configuration of the bridge corresponds to the "ON" state whereas the "DOWN" configuration is associated to the "OFF" one. In order to have good electric performance the impedance matching in the "ON" state is required. In many cases due to technological reasons this result cannot be achieved with just a bridge. Two topologies have been proposed in literature to overcome this problem. The first one, shown in Figure 1, is obtained by adding two equal transmission lines, with suitable values of the characteristic impedance and of the electric length, to the CPW metallic membrane. Another possible structure is composed by two MEMS bridges spaced by a uniform transmission line. For both these two solutions analytic design procedures have been provided in [2, 4], modelling the MEMS device by a simple shunt connected capacitance. However in some cases a more general equivalent circuit should be used for the accurate characterization of the component. This issue has been dealt with in [8], where for the CPW flexible membrane a T-network has been adopted. In this paper, we present a novel method, based on the image parameter representation of two port networks, to improve the microwave matching in the synthesis of the transmission lines depicted in Figure 1. The basic idea was to impose the matching in the "ON" state of the switch by means of the image impedance but unfortunately, with this approach the physical feasibility of the transmission lines is ensured for a limited range of values of the T-network elements, as discussed in [8]. In order to solve this problem, in this contribution the matching condition is imposed by using the image phase.

It is worth noting that the image phase concept has been employed in the past for the design of distributed phase shifters and amplifiers [9–11]. The organization of this paper is as follows. Section 2 deals with the definition of the image parameters and their use to impose the matching condition on a lossless reciprocal and symmetrical two-port network. In Section 3 these results are applied for the development of an analytic model for the MEMS switch in the "ON" state. Section 4 gives a

Received 3 February 2016, Accepted 18 April 2016, Scheduled 3 May 2016

* Corresponding author: Giancarlo Bartolucci (bartolucci@eln.uniroma2.it).

[1] Department of Electronics Engineering, University of Roma Tor Vergata, Roma, Italy. [2] Altran Italia S.p.A., Roma, Italy. [3] Institute for Microelectronics and Microsystems, CNR, Roma, Italy.

comparison with the design method based on the image impedance presented in [8]. Section 5 concerns the experimental characterization of a previously manufactured MEMS coplanar bridge, which is used in this work to provide design examples corresponding to actual devices. In Section 6 numerical results of circuital simulations are illustrated, and considerations on the switch optimization in terms of electric performance and size reduction are discussed. Finally, in Section 7, we summarize some conclusions.

2. THE IMAGE PARAMETER MATCHING CONDITION

For a reciprocal symmetrical lossless two-port network an image impedance Z_i and an image phase ϕ_i can be defined as [12, 13]:

$$Z_i = \sqrt{\frac{B'}{C'}}, \tag{1}$$

$$\cos\phi_i + j\sin\phi_i = \sqrt{AD} + j\sqrt{B'C'} \tag{2}$$

being A, B, C, D the transmission matrix elements and $A = D$, $B = jB'$, $C = jC'$. A, B' and C' are real numbers. According to [9, 11] the scattering parameter S_{11} of the network can be expressed as:

$$S_{11} = \frac{j\left(\frac{B'}{Z_0} - C'Z_0\right)}{2A + j\left(\frac{B'}{Z_0} + C'Z_0\right)} = \frac{j\left(\frac{Z_i}{Z_0} - \frac{Z_0}{Z_i}\right)\sin\phi_i}{2\cos\phi_i + j\left(\frac{Z_i}{Z_0} + \frac{Z_0}{Z_i}\right)\sin\phi_i} \tag{3}$$

Thus the matching condition $S_{11} = 0$ can be fulfilled imposing:

$$Z_i = Z_0 \tag{4}$$

or

$$\phi_i = k\pi \tag{5}$$

with $k = 1, 2, 3, \ldots$.

It can be easily demonstrated that Equation (5) is equivalent to the following condition:

$$B' = C' = 0 \tag{6}$$

A comparison between the use of Equation (5) or Equation (6) will be discussed in another section of this paper.

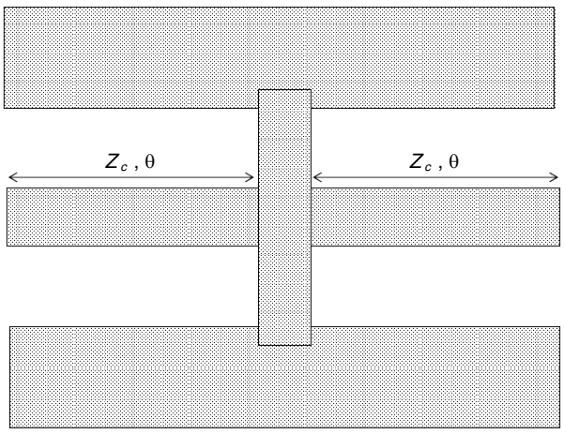

Figure 1. The basic cell composed by the MEMS coplanar bridge and two equal uniform transmission lines.

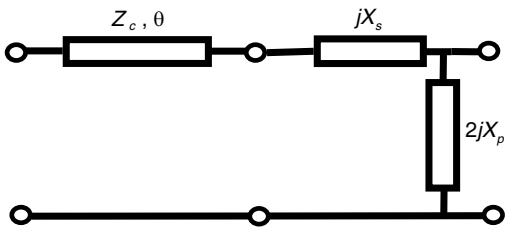

Figure 2. The basic half-cell circuital model obtained replacing the coplanar MEMS bridge by a lossless reciprocal and symmetrical T-network.

3. THE ANALYTIC MODEL WITH THE BRIDGE IN THE "UP" POSITION

As discussed in the introduction, the most critical configuration for the RF MEMS shunt connected switch is with the electrostatically actuated membrane in the "UP" position, resulting often too high reflection values due to some technological mismatch between the designed geometrical values (length, width, ...) and the manufactured ones. Thus, to reduce this drawback improving the matching, the structure in Figure 1 has been proposed and extensively studied. In particular, for such a component, the matching condition has been imposed in [8] by means of Equation (4). In this section Equation (5) will be used to achieve the same result, characterizing the component in terms of the above defined image phase. To this end the proper modeling of the membrane plays a crucial role. A number of papers have been published on this topic in literature [14–19]. Recently a general and accurate equivalent circuit has been developed in [8] for the coplanar bridge in the "up" position. More in detail, neglecting losses, the bridge has been modeled by means of a T-network with two equal series connected X_s reactances and a shunt connected X_p reactance. The values of X_s and X_p can be provided by experimental measurements or by electromagnetic simulations. The same topology is adopted in this paper. Therefore the model of the structure in Figure 1 is obtained by replacing the membrane with its T-network. The symmetry property of this circuit allows analyzing only the half-cell topology depicted in Figure 2. Since the half-cell is a non-symmetric network, for its characterization two image impedances Z_{ihc1} and Z_{ihc2} must be defined together with the image phase ϕ_{ihc}. These parameters are related to the elements of the half-cell transmission matrix as follows:

$$A_{hc} = \cos\phi_{ihc}\sqrt{\frac{Z_{ihc1}}{Z_{ihc2}}} = \left(1+\frac{X_S}{2X_P}\right)\cos\theta + \frac{Z_c}{2X_P}\sin\theta \tag{7}$$

$$B'_{hc} = \sin\phi_{ihc}\sqrt{Z_{ihc1}Z_{ihc2}} = X_S\cos\theta + Z_c\sin\theta \tag{8}$$

$$C'_{hc} = \frac{\sin\phi_{ihc}}{\sqrt{Z_{ihc1}Z_{ihc2}}} = \left(1+\frac{X_S}{2X_P}\right)\frac{\sin\theta}{Z_c} - \frac{\cos\theta}{2X_P} \tag{9}$$

$$D_{hc} = \cos\phi_{ihc}\sqrt{\frac{Z_{ihc2}}{Z_{ihc1}}} = \cos\theta - \frac{X_S}{Z_c}\sin\theta \tag{10}$$

For a well-known property of the image parameter, since two half-cells equal between them compose the basic cell, its image phase ϕ_{ic} is related to ϕ_{ihc} by the formula:

$$\phi_{ic} = 2\phi_{ihc} \tag{11}$$

Two configurations will be considered: the first one utilizes a single basic cell (Figure 1), whereas the second one is realized by the cascaded connection of two basic cells (Figure 3). Thus for the image phases of these two structures we obtain:

$$\phi_i = \phi_{ic} = 2\phi_{ihc} \quad \text{for the single basic cell configuration (Figure 1)} \tag{12}$$

$$\phi_i = 2\phi_{ic} = 4\phi_{ihc} \quad \text{for the double basic cell configuration (Figure 3)} \tag{13}$$

Forcing the phase ϕ_i to the values provided by (5) we have a matched switch when the bridge is in the "up" position. Because of the periodic behavior of the trigonometric functions we shall assume for k the two values $k = 1$, 2, thus writing for ϕ_i:

$$\phi_i = \pi, 2\pi \tag{14}$$

It is important noting that the use of the image phase condition in Equation (5) instead of the transmission matrix element condition in Equation (6) allows a remarkable reduction of the analytic effort. In fact, the calculation of B' and C', even only for the entire single cell is quite intricate. Much worse it is to obtain B' and C' for the double cell configuration, resulting in a long and tedious procedure. Actually, for a network composed by a number of equal basic cells the use of the image parameters provides simple and straightforward mathematical relationships between the representation of the elementary cell and the representation of the entire structure. The latter consideration suggests a further application of the presented approach to another MEMS component. In fact, the topology of a binary distributed phase shifter is basically the same of the double cell switch, and thus (4) and (5) can be used to achieve a non-conventional design methodology for this kind of phase shifter. This aspect will be investigated in future research activity.

In the following part of this section a detailed analysis for the single and double cell switches will be presented.

3.1. The Single Cell Configuration

According to Equations (12) and (14) two cases will be considered:

$$\text{a)} \qquad \phi_i = \phi_{ic} = 2\phi_{ihc} = \pi \quad \Rightarrow \quad \phi_{ihc} = \frac{\pi}{2}$$

Inserting this ϕ_{ihc} value in (7) and (10) we have:

$$A_{hc} = \left(1 + \frac{X_S}{2X_P}\right)\cos\theta + \frac{Z_c}{2X_P}\sin\theta = 0 \tag{15}$$

$$D_{hc} = \cos\theta - \frac{X_S}{Z_c}\sin\theta = 0 \tag{16}$$

After calculation, one may obtain the following relations for the characteristic impedance Z_c and for the electric length of the transmission lines, termed in this case θ_1:

$$Z_c = \sqrt{-X_S\left(X_S + 2X_P\right)} \tag{17}$$

$$\tan\theta_1 = \frac{Z_c}{X_S} \tag{18}$$

$$\text{b)} \qquad \phi_i = \phi_{ic} = 2\phi_{ihc} = 2\pi \quad \Rightarrow \quad \phi_{ihc} = \pi$$

Substituting this ϕ_{ihc} value in Equations (8) and (9), we obtain $B'_{hc} = 0$, $C'_{hc} = 0$, which provide for Z_c the same expression (17). Moreover, for the electric length, defined θ_2, we find:

$$\tan\theta_2 = -\frac{X_S}{Z_c} \quad \Rightarrow \quad \theta_2 = \theta_1 + \frac{\pi}{2} \tag{19}$$

In actual MEMS shunt varactor typically we have:

$$X_S > 0, \quad X_P < 0, \quad |X_S| < |X_P| \quad \Rightarrow \quad -X_S\left(X_S + 2X_P\right) > 0$$

Therefore Z_c is a real number. We can infer from Equation (19) that case a) ($\theta = \theta_1$) requires quite shorter transmission line sections in comparison to case b) ($\theta = \theta_2$), resulting in a remarkable size reduction. Moreover, both the solutions do not allow choosing the characteristic impedance value, being this parameter fixed for given X_s and X_p reactances.

3.2. The Double Cell Configuration

The same procedure used for the single cell configuration will be adopted here. Therefore, according to Equations (16) and (17), two cases will be studied:

$$\text{a)} \qquad \phi_i = 2\phi_{ic} = 4\phi_{ihc} = \pi \quad \Rightarrow \quad \phi_{ihc} = \frac{\pi}{4} \tag{20}$$

Equations (7), (8), (9) and (10) provide the relationship:

$$\sqrt{\frac{B'_{hc}C'_{hc}}{A_{hc}D_{hc}}} = \tan\phi_{ihc} = \sqrt{\frac{\left(X_S + U\right)\left(\dfrac{U}{Z_c^2}\left(1 + \dfrac{X_S}{2X_P}\right) - \dfrac{1}{2X_P}\right)}{\left(1 + \dfrac{X_S}{2X_P} + \dfrac{U}{2X_P}\right)\left(1 - \dfrac{X_S U}{Z_c^2}\right)}} \tag{21}$$

where

$$U = Z_c\tan\theta \tag{22}$$

Imposing in Equation (21) the ϕ_{ihc} value given by Equation (20), after some algebra, the following quadratic equation in the unknown U is obtained:

$$-\frac{U^2}{Z_c^2}\left[\left(1 + \frac{X_s}{X_p}\right)\right] + U\left[\frac{1}{X_p} - \frac{2X_s}{Z_c^2}\left(1 + \frac{X_s}{2X_p}\right)\right] + \frac{X_s}{X_p} + 1 = 0 \tag{23}$$

The solutions of this equation can be written as:

$$U_1 = \frac{\frac{1}{X_p} - \frac{2X_s}{Z_c^2}\left(1+\frac{X_s}{2X_p}\right) - \sqrt{\Delta}}{\frac{2}{Z_c^2}\left[\left(1+\frac{X_s}{X_p}\right)\right]}, \tag{24}$$

$$U_2 = \frac{\frac{1}{X_p} - \frac{2Xs}{Z_c^2}\left(1+\frac{X_s}{2X_p}\right) + \sqrt{\Delta}}{\frac{2}{Z_c^2}\left[\left(1+\frac{X_s}{X_p}\right)\right]} \tag{25}$$

where:

$$\Delta = \left[\frac{1}{X_p} - \frac{2X_s}{Z_c^2}\left(1+\frac{X_s}{2X_p}\right)\right]^2 + \frac{4}{Z_c^2}\left(1+\frac{X_s}{X_p}\right)^2 \tag{26}$$

b) $\phi_i = 2\phi_{ic} = 4\phi_{ihc} = 2\pi \quad \Rightarrow \quad \phi_{ihc} = \frac{\pi}{2}$

This case has been previously studied in the single cell configuration analysis.

4. COMPARISON WITH THE IMAGE IMPEDANCE APPROACH

For the single cell configuration the design of the transmission lines can be even carried out by means of the image impedance method. As it results from [8], with that approach the calculation of the electric length of the lines is achieved by solving a quadratic equation, whose unknown is the same variable U defined in (22). The discriminant Δ_1 of that equation is re-written here for convenience of the reader [8]:

$$\Delta_1 = \left[(X_p+X_s)\left(1-\frac{Z_0^2}{Z_c^2}\right)\right]^2 - 4\left[\frac{1}{2} + \left(X_p+\frac{X_s}{2}\right)X_s\frac{Z_0^2}{Z_c^4}\right]\left[\left(X_p+\frac{X_s}{2}\right)X_s + \frac{Z_0^2}{2}\right] \tag{27}$$

We can note that, since it could be $\Delta_1 < 0$, the image impedance approach does not always ensure the existence of the problem solution. A similar event occurs even for the single cell topology, by using the image phase matching method, because of the technological limits on the characteristic impedance values. Conversely, for the above studied double cell configuration the condition $\Delta > 0$ is always fulfilled, and furthermore the designer can choose the Z_c value. For this case, from (26), we find:

$$\left|\frac{1}{X_p} - 2\frac{X_s}{Z_c^2}\left(1+2\frac{X_s}{X_p}\right)\right| < \sqrt{\Delta} \tag{28}$$

Since the denominator of Equations (24) and (25) is typically a positive number, it can be inferred that in most cases $U_2 > 0$ and $U_1 < 0$, being otherwise $U_2 < 0$ and $U_1 > 0$. Thus, in conclusion, the image phase approach applied to the double cell configuration always provides a feasible solution of the design problem, irrespective of the X_s and X_p values.

5. CHARACTERIZATION OF THE REALIZED MEMS BRIDGE

Microwave MEMS shunt coplanar varactors typically include a thin flexible metal bridge which is suspended across the central conductor of the transmission line and is electrostatically actuated. In [20] the authors have recently presented a novel process based on SU-8 for the fabrication of MEMS shunt capacitive devices. SU-8 is a negative photoresist, and has been used both for the lateral supports for the suspended membrane and as sacrificial layer. In that paper [20] all the technological aspects concerning the fabrication of such a component have been discussed, and therefore for sake of brevity will not be presented here again. The final structure is depicted in Figure 4. We can note that transmission line sections are added to the coplanar bridge to characterize the MEMS device by means of microwave probes connected to a network analyzer. Since the characteristic impedance of these coplanar lines is 50 ohm their presence does not affect the magnitude of the scattering parameters. The frequency

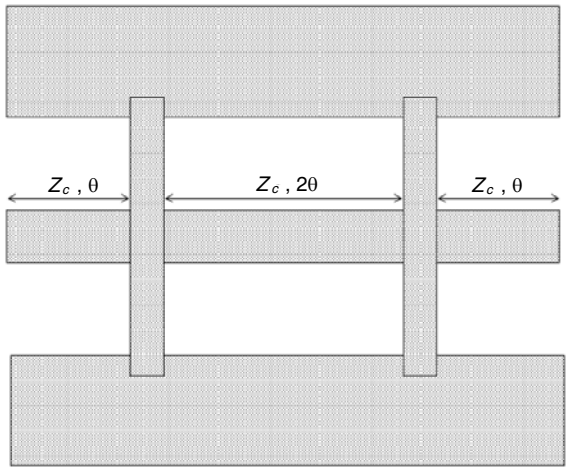

Figure 3. The double basic cell configuration.

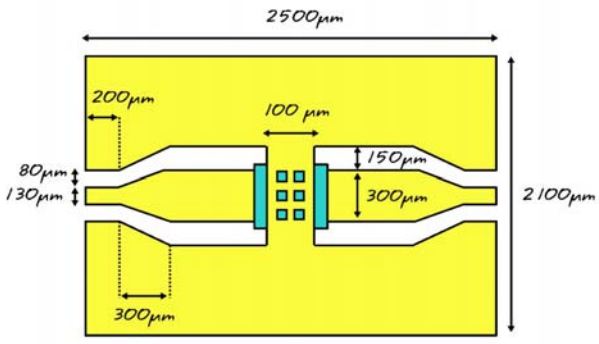

Figure 4. Schematic of the RF MEMS bridge.

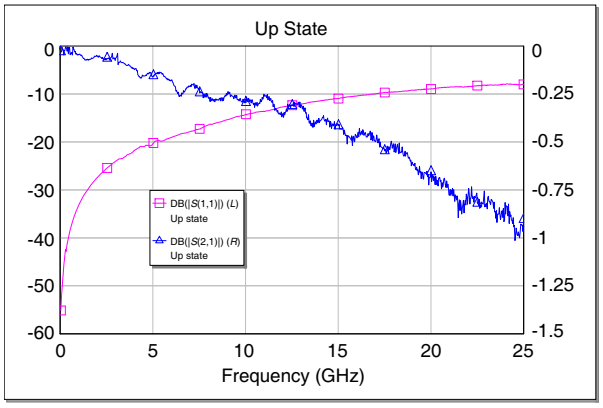

Figure 5. Magnitude of the S_{11} and S_{21} parameters with the bridge in the UP state.

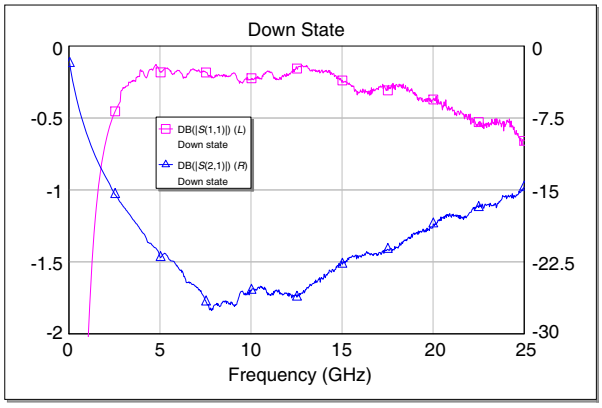

Figure 6. Magnitude of the S_{11} and S_{21} parameters with the bridge in the DOWN state.

behaviors of the measured $|S_{11}|$ and $|S_{21}|$ are plotted in Figures 5 and 6 for the membrane in the up and down position respectively. In particular, from these experimental results we can infer that for frequency values higher than 10 GHz the device in the ON state exhibits high reflection losses. To solve this problem the above developed approach will be used in the next section for the synthesis of the matching transmission lines.

6. DESIGN CONSIDERATIONS, SIMULATION RESULTS AND DISCUSSION

The first step of the design procedure of the switch is to choose the central operating frequency f_0. We assume $f_0 = 20$ GHz. According to the described analytic model, the second step is to obtain the X_s and X_p values at f_0 for the MEMS coplanar bridge in the UP position. In order to remove the effects of the 50 ohm coplanar lines from the X_s and X_p reactances a simple de-embedding method can be used, shifting the reference planes of a distance corresponding to the electric length of these transmission lines. More in detail, as shown in Figure 4, the bridge is inserted between two 50 ohm lines, each one with a geometric length of 1200 μm, that is 72.6° at f_0. Therefore, the phase of each scattering parameter measured at f_0 has been changed by adding 145.2°. The so obtained scattering parameters are used in the conversion relations from S matrix to Z matrix, having eventually the following values for X_s and X_p: $X_s = 3.4\,\Omega$, $X_p = -56.6\,\Omega$. These reactances must be inserted in the synthesis equations derived in Section 3 for the single and double cell configurations.

6.1. The Single Cell Configuration

By substituting the achieved X_s and X_p reactances in Equations (17) and (18) we find $Z_c = 19.3\,\Omega$ and $\theta_1 = 80°$. It is worth noting that such a characteristic impedance value is not easy to realize in coplanar technology [21, 22]. As discussed above, in addition to this first case, another single cell structure should be considered. The second solution employs transmission line sections with the same characteristic impedance value Z_c of the first case, and electric length θ_2 given by Equation (19): $\theta_2 = 170°$. Both the structures have been simulated by means of the software package AWR Microwave Office, using a black box model for the MEMS bridge in the up position, in which the de-embedded scattering parameters are inserted. The model is obtained by subtracting from the measured data the effect of an input line and an output line with 50 ohm characteristic impedance and electrical length 72.6° at f_0, that is adding two lines with negative lengths. The behaviors of the reflection coefficient amplitudes versus frequency are shown in Figure 7, where case 1 corresponds to the electric length θ_1 and case 2 corresponds to θ_2. Satisfactory values for S_{11} are obtained at f_0 for case 2, although the switch appears to be too long. The other structure (case 1) is quite shorter, but exhibits not adequate values for the reflection coefficient.

6.2. The Double Cell Configuration

By using the above given extracted reactances X_s and X_p, the denominator of Equations (24) and (25) is a positive number, and therefore, according to the results of Section 4, we obtain: $U_1 < 0$, $U_2 > 0$. Let us assume for the characteristic impedance Z_c a range from $50\,\Omega$ to $90\,\Omega$. In order to have a short component we shall adopt the solutions with $\theta < \pi/2$. Hence, for the physical realization of the

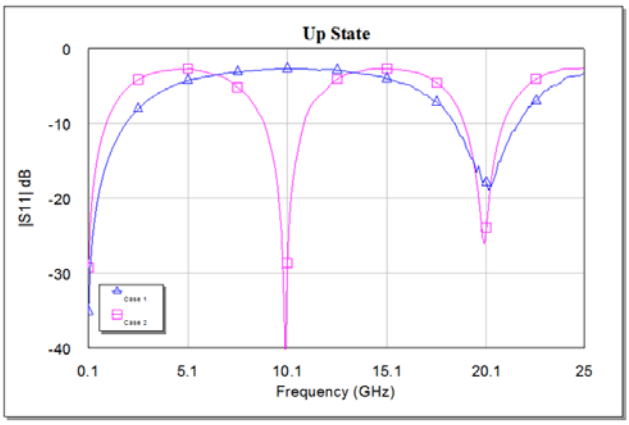

Figure 7. Magnitude of the S_{11} parameter with the bridge in the UP position for two single cell configurations corresponding respectively to the electric length values θ_1 (case 1) and θ_2 (case 2).

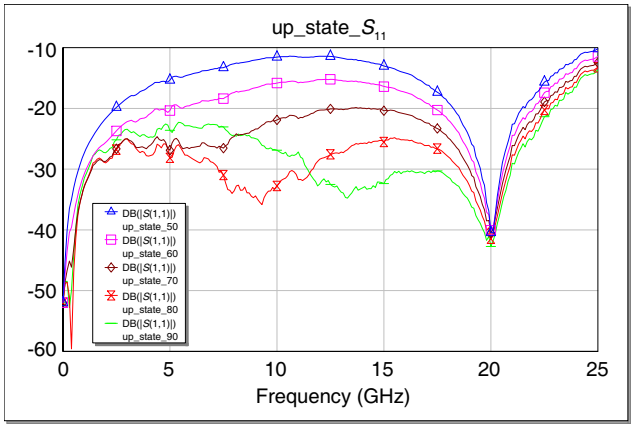

Figure 8. Magnitude of the S_{11} parameter with the bridge in the UP position (ON state) for different double cell configurations. Five cases are considered, characterized by the Z_c and θ values reported in Table 1.

Table 1. Characteristic impedance Z_c of the double switch configuration and corresponding electrical lengths of the uniform line sections.

Z_c (ohm)	θ (degrees)
50	30.8
60	29
70	27.3
80	25.7
90	24.2

structure U must be a positive number. Consequently, only U_2 can be chosen. The electric lengths θ, computed by means of Equation (22), are summarized in Table 1 for different values of the characteristic impedance Z_c. The results of the simulations of these five switches, performed by AWR Microwave Office utilizing the previously presented black box model for the MEMS membrane in the on configuration, are illustrated in Figures 8 and 9. In particular, the amplitude of S_{11} as a function of frequency is plotted in Figure 8 for characteristic impedance values ranging from $50\,\Omega$ to $90\,\Omega$. The amplitude of S_{21} is shown in Figure 9. For sake of completeness for the switch in the OFF state the isolation ($|S_{21}|$) versus frequency is presented in Figure 10. These last behaviors have been obtained using the same procedure adopted for the simulation of the switch in the ON state, but inserting in the black box model the de-embedded measured scattering parameters for the bridge in the down position.

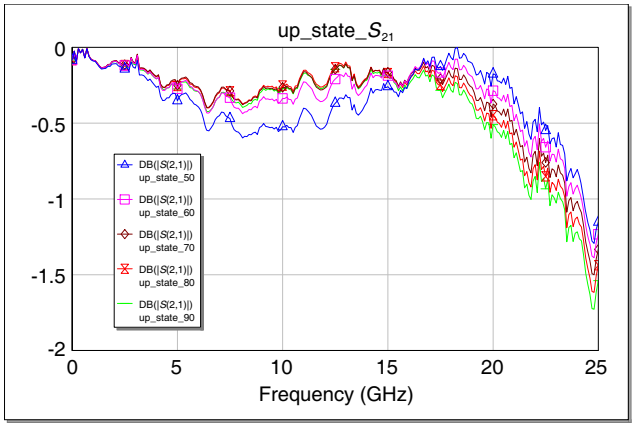

Figure 9. Magnitude of the S_{21} parameter with the bridge in the UP position (ON state) for different double cell configurations. Five cases are considered, characterized by the Z_c and θ values reported in Table 1.

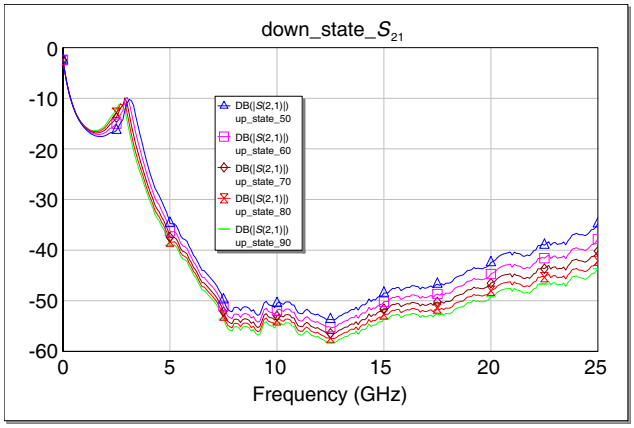

Figure 10. Isolation (magnitude of S_{21} with the bridge in the DOWN position, OFF state) for different double cell configurations. Five cases are considered, characterized by the Z_c and θ values reported in Table 1.

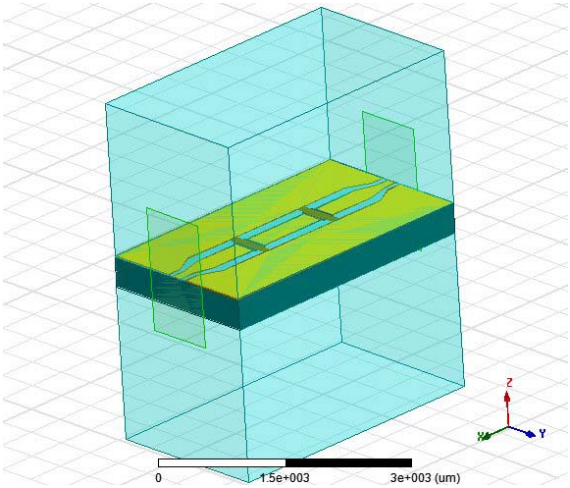

Figure 11. Layout of the double cell switch ($Z_c = 50\,\Omega$) in the ON state for the electromagnetic simulation by means of the Ansoft HFSS 3D software package.

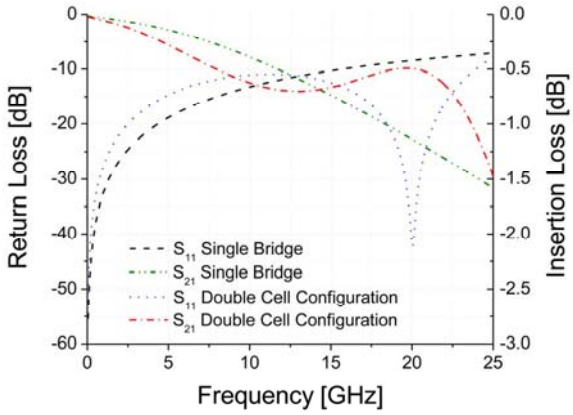

Figure 12. Behaviour of $|S_{11}|$ and $|S_{21}|$ versus frequency for the switch in the on state. The Ansoft HFSS 3D software package has been used for the electromagnetic simulation of the MEMS single bridge structure and of the double cell configuration with $Z_c = 50\,\Omega$.

The main considerations suggested by the presented results can be summarized as follows:

- increasing the characteristic impedance Z_c the electric length θ decreases;
- in the ON state the switch exhibits a broadband frequency behavior for the S_{11} parameter for $Z_c > 80\,\Omega$;
- in the OFF state high isolation values are obtained;
- The choice of $Z_c = 50\,\Omega$ allows to have a remarkable size reduction. In fact, the external transmission line sections are not needed. Hence, neglecting the bridge contribution to the overall size of the switch, the electric length of the component is halved, in comparison with the other possible solutions, passing from 4θ to 2θ. Moreover, there is no discontinuity due to the presence of an impedance change from Z_c to Z_0 and therefore of a step in width in the central conductor or in the lateral ground planes of the coplanar waveguide. In order to check the validity of the presented approach the structure with $Z_c = 50\,\Omega$ has been simulated in the ON state by means of the Ansoft HFSS 3D electromagnetic simulator. The box with the layout of the double cell switch is depicted in Figure 11. Numerical values are shown in Figure 12, where $|S_{11}|$ and $|S_{21}|$ are plotted as a function of the frequency even for the case of the single MEMS coplanar bridge. A good agreement with the results in Figures 5, 8 and 9 has been obtained.

6.3. Final Discussion

In this part of the paper, we shall present a final discussion on the structures proposed for the solution of the design problems of the MEMS shunt capacitive switches. The first step is to compare the coplanar single bridge configuration with the double bridge one. It is obvious that the use of only one MEMS device is an important advantage. However, the single bridge component exhibits poor electric performance together with a total length of the transmission line sections quite higher than that one needed for the double bridge structure. Therefore, in our opinion the single bridge configuration is not suitable for the realization of the switch. For the other topology, two different solutions can be adopted. The first one is characterized by $Z_c = 50\,\Omega$. In this case, the main advantage is the remarkable reduction of the size. An alternative possibility is to use a high value for the characteristic impedance ($Z_c > 80\,\Omega$), obtaining a quite short component with very good electric performance in terms of reflection losses frequency behavior.

7. CONCLUSION

In this paper, it has been described as a novel approach to analytically design the transmission line sections used in RF MEMS shunt switches to have a matched component in the "ON" state. The method is based on the image parameter characterization of the switch. In particular, the image phase has been utilized to impose the matching condition. Two topologies, characterized by a different number of basic cells, have been studied. Original closed-form expressions for the synthesis of the component have been given. Experimental data of a previously realized MEMS coplanar bridge have been used to produce design examples. A detailed discussion on these results has been presented. The effectiveness of the proposed approach has been finally demonstrated.

REFERENCES

1. Muldavin, J. B. and G. M. Rebeiz, "High-isolation CPW MEMS shunt switches — Part 1: Modeling," *IEEE Trans. Microwave Theory Tech.*, Vol. 48, No. 6, 1045–1052, Jun. 2000.
2. Muldavin, J. B. and G. M. Rebeiz, "High-isolation CPW MEMS shunt switches — Part 2: Design," *IEEE Trans. Microwave Theory Tech.*, Vol. 48, No. 6, 1053–1056, Jun. 2000.
3. Rizk, J., G. L. Tan, J. B. Muldavin, and G. M. Rebeiz, "High-isolation W-band MEMS switches," *IEEE Microwave and Wireless Components Letters*, Vol. 11, No. 1, 10–12, Jan. 2001.
4. Rebeiz, G. M., *RF MEMS: Theory, Design, and Technology*, John Wiley & Sons, Hoboken, New Jersey, USA, 2003.

5. Zheng, W. B., Q. A. Huang, X. P. Liao, and F. X. Li, "RF MEMS membrane switches on GaAs substrates for X-band applications," *Journal of Microelectromechanical Systems*, Vol. 14, No. 3, 464–471, Jun. 2005.
6. Shen, Q. and N. Scott Barker, "Distributed MEMS tunable matching network using minimal-contact RF-MEMS varactors," *IEEE Trans. Microwave Theory Tech.*, Vol. 54, No. 6, 2646–2658, Jun. 2006.
7. Domingue, F., S. Fouladi, A. B. Kouki, and R. R. Mansour, "Design methodology and optimization of distributed MEMS matching networks for low-microwave-frequency applications," *IEEE Trans. Microwave Theory Tech.*, Vol. 57, No. 12, 3030–3041, Dec. 2009.
8. Bartolucci, G., G. de Angelis, A. Lucibello, R. Marcelli, and E. Proietti, "Analytic modeling of RF MEMS shunt connected capacitive switches," *Journal of Electromagnetic Waves and Applications*, Vol. 26, Nos. 8–9, 1168–1179, 2012.
9. Bartolucci, G., "Image parameter modeling of analog traveling-wave phase shifters," *IEEE Transactions on Circuits and Systems I: Fundamental Theory and Applications*, Vol. 49, No. 10, 1505–1509, Oct. 2002.
10. Bartolucci, G., S. Catoni, F. Giacomozzi, R. Marcelli, B. Margesin, and D. Pochesci, "Realisation of distributed RF MEMS phase shifter with very low number of switches," *Electronics Letters*, Vol. 43, No. 23, 1290–1292, Nov. 2007.
11. Bartolucci, G., F. Giannini, and L. Scucchia, "Design considerations for the gate circuit in distributed amplifiers," *IET Circuits, Devices and Systems*, Vol. 4, No. 3, 181–187, May 2010.
12. Pozar, D. M., *Microwave Engineering*, 2nd Edition, Wiley, New York, 1998.
13. Matthaei, G., L. Young, and E. M. T. Jones, *Microwave Filters, Impedance-matching Networks, and Coupling Structures*, Artech House, Norwood, MA, United State of America, 1980.
14. Puyal, V., D. Dragomirescu, C. Villeneuve, J. Ruan, P. Pons, and R. Plana, "Frequency scalable model for MEMS capacitive shunt switches at millimeter-wave frequencies," *IEEE Trans. Microwave Theory Tech.*, Vol. 57, No. 11, 2824–2833, Nov. 2009.
15. Bartolucci, G., R. Marcelli, S. Catoni, F. Giacomozzi, B. Margesin, V. Mulloni, and P. Farinelli, "An equivalent-circuit model for shunt-connected coplanar microelectromechanical — System switches for high frequency applications," *Journal of Applied Physics*, Vol. 104, 845141–845148, Oct. 2008.
16. Vähä-Heikkilä, T., K. van Caekenberghe, J. Varis, J. Tuovinen, and G. M. Rebeiz, "RF MEMS impedance tuners for 6–24 GHz applications," *International Journal of RF and Microwave Computer-Aided Engineering*, Vol. 17, No. 3, 265–278, May 2007.
17. Halder, S., C. Palego, Z. Peng, J. C. M. Hwang, D. I. Forehand, and C. L. Goldsmith, "Compact RF model for transient characteristics of MEMS capacitive switches," *IEEE Trans. Microwave Theory Tech.*, Vol. 57, No. 1, 237–242, Jan. 2009.
18. Marcelli, R., G. Bartolucci, G. Minucci, B. Margesin, F. Giacomozzi, and F. Vitulli, "Lumped element modelling of coplanar series RF MEMS switches," *Electronics Letters*, Vol. 40, No. 20, Sep. 2004, 1272–1274.
19. Peroulis, D., S. P. Pacheco, and L. P. B. Katehi, "RF MEMS switches with enhanced power-handling capabilities," *IEEE Trans. Microwave Theory Tech.*, Vol. 52, No. 1, 59–68, Jan. 2004.
20. Lucibello, A., E. Proietti, F. Giacomozzi, R. Marcelli, G. Bartolucci, and G. de Angelis, "RF MEMS switches fabrication by using SU-8 technology," *Microsystem Technologies*, Vol. 19, No. 6, 929–936, Jun. 2013.
21. Goyal, R., *Monolithic Microwave Integrated Circuits: Technology and Design*, Artech House, Norwood, MA, United State of America, 1989.
22. Simons, R., *Coplanar Waveguide Circuits, Components, and Systems*, Wiley, New York, 2001.